Degradation Assessment for Prototypal Perovskite Photovoltaic Modules in Long Term Outdoor Experimental Campaign

Degradation Assessment for Prototypal Perovskite Photovoltaic Modules in Long Term Outdoor Experimental Campaign

Giona Aime
Dip. Energia "G. Ferraris"
Politecnico di Torino
Corso Duca Abruzzi 24, Torino, Italy
giona.aime@studenti.polito.it

Stéphanie Narbey
Solaronix SA
Rue de l'Ouriette 129, 1170-Aubonne, Switzerland stephanie.narbey@solaronix.com

Alessandro Ciocia
Dip. Energia "G. Ferraris"
Politecnico di Torino
Corso Duca Abruzzi 24, Torino, Italy alessandro.ciocia@polito.it

Luca Saglietti
Edison Spa
via Paolo Borsellino 38/16, Torino, Italy
luca.saglietti@edison.it Gabriele Malgaroli
Dip. Energia "G. Ferraris"
Politecnico di Torino
Corso Duca Abruzzi 24, Torino, Italy gabriele.malgaroli@polito.it

Filippo Spertino
Dip. Energia "G. Ferraris"
Politecnico di Torino
Corso Duca Abruzzi 24, Torino, Italy
filippo.spertino@polito.it

Abstract— In the future, PhotoVoltaic (PV) modules might overcome the current efficiencies by including crystalline silicon layers and layers of different materials, with different absorption properties. One of the most promising materials to reach this goal is the perovskite, an organic material capable to absorb radiation with wavelength between ≈ 300 nm and ≈ 800 nm. However, the major issue of such a material is its stability over time, as well as the stability of the electrical performance of Perovskite Solar Cells (PSCs). This work investigates the degradation of the electrical performance at Standard Test Conditions (STC) of 4 PSCs using data collected in an experimental campaign carried out in 2022 at Torino (Italy). Since these modules were prototypes, their electrical performance at STC was determined in the first day of the campaign. In addition, the degradation of maximum power and efficiency over time was investigated. Finally, the temperature coefficients for power were estimated in the first day of the campaign.

Keywords—perovskite solar cells, degradation, outdoor testing, long term experimental campaign, temperature coefficients.

I. INTRODUCTION

In the recent years, the global energy demand has significantly grown, and the adoption of generators based on Renewable Energy Sources (RES) is increasing due to their reduced polluting emissions. In this context, PhotoVoltaic (PV) technology is the most diffused because it is clean [1], reliable as it requires low maintenance [2]. In addition, wind turbines [3] or other renewable generators [4] can be integrated in complex systems [5] like energy communities [6] to increase the self-sufficiency of the users or to optimize the exploitation of renewable energy. PV technologies can consist of different materials [7]: crystalline silicon (c-Si), amorphous silicon (a-Si), or thin films. Such technologies permit to achieve efficiencies up

to ≈26% in commercial PV modules [8]. The current challenges in the PV sector at the European level consist in increasing the modules' conversion efficiency and limiting their manufacturing cost. However, in the last decade, the performance improvement of the most efficient technology (monocrystalline silicon, m-Si) was limited [9].

The integration of other materials capable of absorbing different wavelengths of solar radiation is currently under investigation [10]. In this context, one of the most promising materials is based on the perovskite [11]. Such a material has a crystalline structure ABX_3, where A is the organic cationic group, B represents the inorganic cationic group and X indicates the halogen ionic groups [11]. Nowadays, the most widely used perovskitic technology is the lead halide one [12], in which the organic cation A is the methylammonium ion, $CH_3NH_3^+$, the inorganic cation B is the lead ion, Pb_2^+, and the inorganic cation group X is the tri-hydride ion, I^-. The overall formula is therefore $CH_3NH_3PbI_3$ and this compound is named Methyl-Ammonium-Lead-Tri-Hydride, $MAPbI_3$ [13]. The advantages of these devices are the following. According to their modularity, Perovskite Solar Cells (PSCs) can be integrated in PV modules consisting of different materials, with different absorption properties. Indeed, such cells may consist of perovskite layers merged with other materials (e.g., crystalline silicon). Such configuration may enhance the absorption of solar radiation, increasing the conversion efficiency of the solar modules [14]. PSCs can absorb radiation with wavelength between ≈ 300 nm and ≈ 800 nm [15]: however, this wavelength range is much narrower than silicon cells, which can absorb radiation up to about 1200 nm [16]. Hence, it is fundamental to extend the absorption range of PSCs [17]. Current values of energy gaps for PSCs are about 1.4 eV [18], which increase with temperature, permitting to achieve efficiencies up to about 18%. Moreover, the diffusion length of the carriers ranges between ≈ 100 nm and a few μm, permitting to limit the layers thickness, which is much lower than c-Si wafers [19]. In addition, perovskite is a synthetic material with a lower manufacturing cost than c-Si [20]. The major issue with such a material is its stability over time, as well as the stability of its electrical performance [21]. On the contrary, the performance of Si modules is, generally, guaranteed to be higher than 80% of its rated value after 20 or more years [22]. The degradation of PSCs might be due to factors like the instability of organic materials, fast variations of operating conditions (e.g., fast variations of environmental parameters like irradiance, air temperature, wind speed, relative humidity), and not optimal insulation [23]. Thus, it is important to define standard tests and analyses aiming to quantify this degradation effect and to compare the performance of different PSCs. In this context, some testing protocols, named ISOS [24], were defined at the International Summit on Organic PV Stability. Such protocols were grouped in five categories: dark storage testing, light-soaking testing, outdoor testing, thermal cycling testing and light-humidity-thermal cycling testing. The outdoor testing is the most important to investigate the electrical performance of the perovskite cells in real operating conditions, as well as its degradation over time. The ISOS-O protocols are three [25]: the ISOS-O-1, in which periodic measurements of the current-voltage (*I-V*) curves are performed by a sun simulator; the ISOS-O2, in which the cells work in the neighbourhood of their Maximum Power Point (MPP) and their *I-V* curves are traced under sunlight; the ISOS-O-3, in which the PSCs operate at their MPP, and their performance is determined under sunlight and under sun simulator both. In this work, the degradation of the electrical performance for four PSCs was determined using ad-hoc ISOS-O-2 protocols in an experimental campaign with long duration. In particular, different protocols were used for each module to evaluate their impact on the performance degradation. In addition, the temperature coefficients of the modules were determined by investigating their performance in an early degradation-free period.

The paper is organised as follows: in Section II, the measurement station used to monitor the performance of the PSCs under test and to store the most important environmental and electrical parameters is described. In Section III, the testing protocols applied to the modules under test are presented. Section IV describes the procedure used to identify the temperature coefficients for power of the tested PSCs, which are presented in section V. Section VI presents the results of the analyses, while section VII contains the conclusions.

The authors gratefully acknowledge the contributions of Swiss company Solaronix SA, for providing the perovskite modules tested in the experimental campaign and analysed in the present work.

II. Description of the Measurement Station

A measurement station was installed by the Italian company Edison on the roof of the Energy Center building (Torino, Italy) under the supervision of the Energy Department of Politecnico di Torino. Such a system was designed to monitor the performance of PV modules in experimental campaigns with long duration (up to years). In particular, in its current configuration, the system consists of the following components:

- 4 programmable electronic loads with maximum power of 60 W (maximum voltage = 60 V, and maximum current = 1 A). These devices have a resolution of 16 bits, and relative uncertainty up to ±0.15% (voltage) and ±0.25% (current). Each electronic load is connected to one PV module, and it acquires the voltage and current signals.
- 4 PT100 sensors with resolution of 0.1 °C, and relative uncertainty < ±0.3 °C measure the temperature of the PV modules on their rear side.
- A spectrally flat class A pyranometer (measurement range 0−2000 W/m^2 and relative uncertainty of ±20 W/ m^2) acquires the incident solar irradiance *G*.
- A weather station includes an anemometer to measure the wind speed (resolution of 0.01 m/s and relative uncertainty of ±1%) and its direction (resolution 0.1° and relative uncertainty of ±1%), a piezoresistive sensor to measure the atmospheric pressure (resolution of 0.1 mbar, relative uncertainty of ±0.4 mbar), one PT100 sensor to measure the ambient temperature (resolution of 0.1 °C, relative uncertainty < ±0.3 °C), and a capacitive sensor to measure the relative humidity (resolution of 0.1%, relative uncertainty of ±2.5%).
- A Personal Computer (PC) runs the control software in LABVIEW ambient to store the acquired quantities in a database.

Fig. 1 presents the schematic with the components of the measurement station.

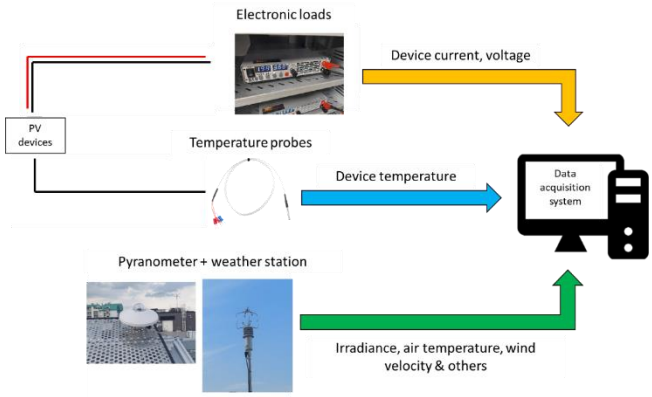

Fig. 1. Components of the measurement system.

III. Testing Protocol of the System

The working principle of the station is presented in Fig. 2. At the beginning of the experimental campaign, the electronic loads are initialized, and their Maximum Power Point Tracking (MPPT) function is activated. In such a state, the loads keep the PV modules working in the neighbourhood of their MPP for a time selected by the user. In addition, periodically, the loads acquire the *I-V* curves of the modules under test, behaving like a resistor with variable resistance. The resistance can vary from zero (modules in short circuit state) to a very high value (modules almost in their open circuit state): hence, the *I-V* curves of PV modules can be measured in reverse voltage (from open circuit to short circuit) or in forward voltage (from short circuit to open circuit).

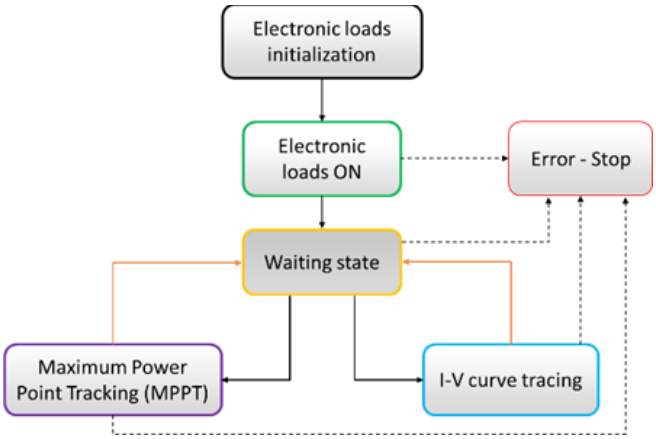

Fig. 2. Principle of operation of the measurement system.

The experimental campaign was based on the repetition over a cycle consisting of two stages: the MPP and the *I-V* curve phases. Their duration was equal to 12 min and 130 s, respectively. The main characteristics of these stages were the following:

- Four MPP searches were performed in the MPP stage.
- The duration of each MPP search was equal to 5 s.
- After the identification of the MPP, the modules were kept at their operating point for 175 s.
- The duration of the *I-V* curve phase was 130 s. However, the duration of the *I-V* tracing was different according to the module under test. In particular, the *I-V* curves were acquired in 130 s for PV modules #1 and #2, while the curves of module #3 were measured in 30 s. In this case, such a module was kept working at its MPP for the remaining 100 s. The curves of these generators were acquired in reverse voltage mode. Finally, two subsequent acquisitions of the *I-V* curves for PV generator #4 were performed: one in reverse voltage mode and one in forward voltage mode. The duration of each acquisition was 65 s.

Fig. 3 presents the different stages of a cycle, as well as the durations of their substages.

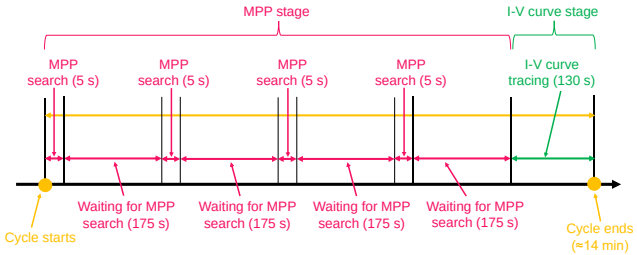

Fig. 3. Duration of the different stages of each cycle.

IV. Evaluation of Temperature Coefficients

The temperature coefficients for power (γ) were identified using nonlinear optimization. The procedure used to determine such coefficients consists in three steps.

First, the *I-V* curves measured under sunny conditions (irradiance higher than 550 W/m^2) were selected. Then, the curves acquired under unstable weather conditions were removed. The Normalized Root Mean Square Error (*NMRSE*) was computed for irradiance and modules temperature. These indexes were computed in the following way:

$$NRMSE_x = 100 \cdot \frac{1}{x_m} \cdot \sqrt{\frac{\sum_{i=1}^{N}(x_m - x_i)^2}{N-1}} \quad (1)$$

where x is the measured generic quantity, x_m is its average value, x_i is the i^{th} quantity value, and N is the number of measurements in a specific time interval. In this work, *I-V* curves measured with normalised root mean square errors on irradiance ($NRMSE_G$) or on module temperature ($NRMSE_T$) higher than 2% and 3%, respectively, were removed. In addition, measurements with wind speed > 5 m/s were excluded as well. In the third step, a nonlinear fitting was carried out to identify the temperature coefficients. The fitting is performed on the following equation:

$$P_{max} = P_{STC} \cdot \frac{G}{G_{STC}} \cdot [1 + \gamma \cdot (T_m - T_{STC})] \qquad (2)$$

where G is solar irradiance, G_{STC} is the irradiance at STC (1000 W/m^2), T_m is the module temperature, T_{STC} is the module temperature at STC (25°C), and P_{STC} is the maximum power at STC.

V. PV Modules under Test

Four perovskite modules, manufactured by the Swiss company Solaronix SA, were tested in an experimental campaign carried out between October 11th and December 21st, 2022 at Torino (latitude of 45° North). Such devices consist of 12 series-connected cells, with a module active area of 56.3 cm^2 each and a glass structure. Fig. 4 presents a picture of the modules on the supporting structure of the measurement station.

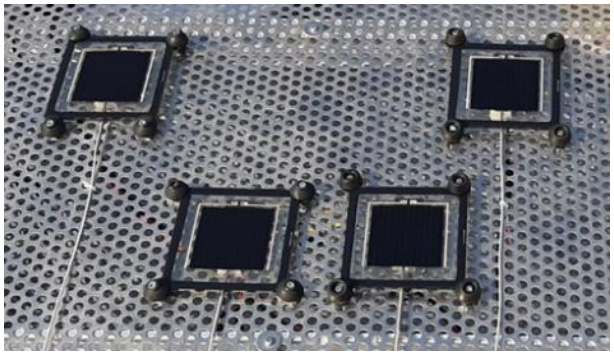

Fig. 4. PSCs under test.

Since they were prototypal modules, their rated power and efficiency at STC (P_{STC}, and η_{STC}, respectively) were not provided by the manufacturer, and they were determined in the first day of the experimental campaign by correcting measured data to STC. In addition, the temperature coefficients of the modules were unknown.

VI. Results

This section presents the results of the experimental campaign. The first result regards the evaluation of the most important electrical parameters at STC. Therefore, in the first day of the campaign, the modules were exposed to sunlight in the hours with the irradiance peak to determine the parameters at STC. However, after measuring the power and efficiency of the PV modules, their correction to STC needed the knowledge of the temperature coefficients γ. These values would not be necessary if the curves were acquired with modules temperature close to STC (25°C). Hence, the measurements were carried out while cooling the modules to obtain modules temperature almost equal to 25°C. Thus, the measured power and efficiency were corrected to STC using equation (2) and neglecting the temperature dependence. The results are presented in Table I: although the modules were prototypes, the manufacturing process was sufficiently mature to obtain comparable performance among the lot of the considered modules.

TABLE I. Measured Maximum Power and Efficiency at STC

PV modules	**P_{STC}**	**η_{STC}**
#1	0,814 W	14,3 %

#2	0,816 W	14,5 %
#3	0,814 W	14,6 %
#4	0,812 W	14,2 %

These measurements, with modules' temperature = 25°C, were periodically performed in clear sky days to compare the performance at STC of the modules at different stages of the campaign. Then, the data from the experimental campaign were processed to assess the degradation of the modules over time, and their temperature coefficients as well.

First, a preliminary filtering of the *I-V* curves was performed to remove measurements affected by mismatch, measurement errors or other issues. In this case, about 20% of acquired curves were removed. Then, the degradation of efficiency was investigated by comparing the STC electrical parameters at the beginning and at the end of the campaign. Such parameters were identified starting from the periodic measurements carried out with modules' temperature = 25°C.

Figures 5 and 6 present the profiles of the maximum power and efficiency at STC over the experimental campaign. The figures include experimental data measured under sufficiently high irradiance (> 550 W/m^2) and corrected to STC. The green dots represent measurements performed with modules' temperature of 25°C and corrected to STC using the irradiance-proportional part of equation (2). On the contrary, blue dots are measurements acquired with modules' temperature different from STC: these data were corrected according to real irradiance and temperature using the coefficients obtained with the procedure described in Section IV. Table II reports the temperature coefficients for the modules under test that were estimated starting from the data acquired in the first day of the campaign. Measurements in the first day were selected to avoid experimental data affected by degradation.

TABLE II. ESTIMATED TEMPERATURE COEFFICIENTS FOR POWER

Module	**γ**
#1	-0.407 %/°C
#2	-0.351 %/°C
#3	-0.245 %/°C
#4	-0.334 %/°C

As previously mentioned, the modules under test present similar initial performance, but the degradation of the modules is different over the campaign. The lowest loss of performance at the end of the campaign occurs for PV module #3 (power reduction of -17.5%), which was tested by measuring its *I-V* curves in the lowest time interval (30 s). On the contrary, the highest degradation rate is for module #4 (power reduction of -51.4%). This module was subject to the highest stress with respect to the others since its *I-V* curves were measured in two directions (forward voltage and reverse voltage). The other two modules present comparable degradation (power reduction of -35.7% and -29.5% for PV modules #1 and #2, respectively). Regarding the efficiency, its profiles over time have the same shape of the maximum power ones. Indeed, at the beginning of the tests, the values of efficiency were comparable and in the range from 14.2% (#4) to 14.6% (#3), while, at the end of the campaign, it ranged between 6.90% (#4) and 12.0% (#3). Finally, the identified γ coefficients were comparable with the values generally provided for the c-Si module (from -0.5 %/°C to - 0.3 %/°C), but they were significantly different for the modules under test. This means that, in the calculation of energy production, the error linked to the thermal losses might be remarkable.

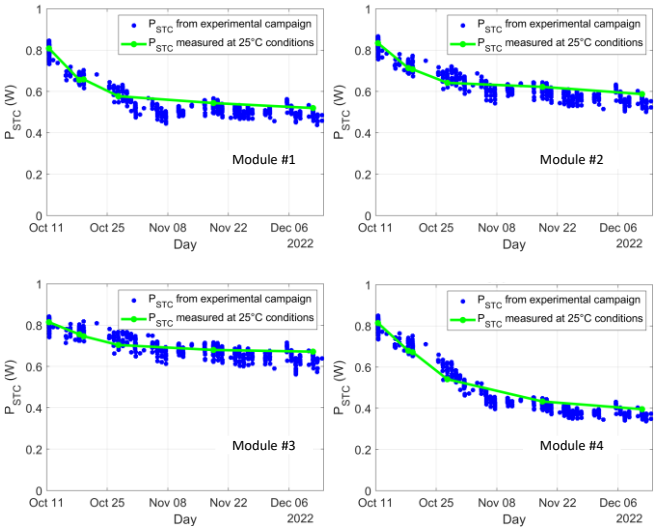

Fig. 5. Maximum power evolution over time for the modules under test.

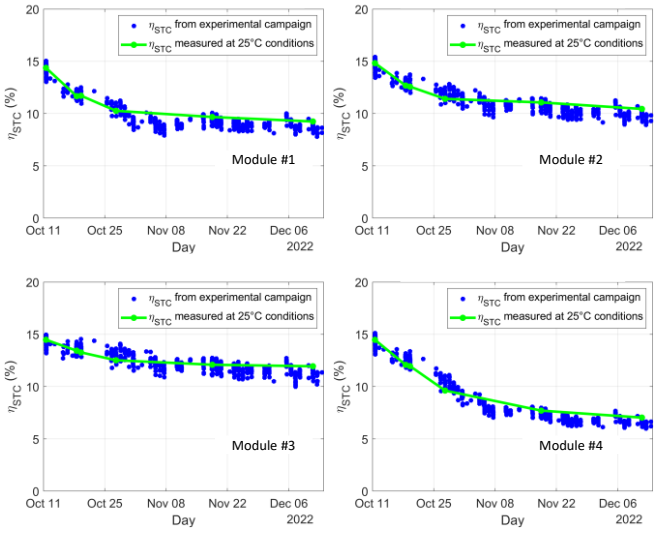

Fig. 6. Efficiency evolution over time for the modules under test.

The best performance with temperature was stated for module #3, which also had the lowest degradation at the end of the campaign. Finally, the assumption of no degradation during the first day of the campaign was confirmed by Figures 5 and 6. Actually, the blue dots (measurements corrected to STC using the temperature coefficients) and the green dots (data obtained at 25 °C by cooling the modules and corrected using the irradiance-proportional part of equation (2)) almost overlap. This behaviour states that the temperature coefficients did not change during the experimental campaign. These results confirm that perovskite cells still need technological improvements to allow installations for commercial application. However, their potential to increase the efficiency of PV modules with respect to conventional c- Si modules is clear. In this context, further experimental campaigns on new prototypal devices with larger surface, and so higher maximum power, will be conducted in the future.

VII. Conclusions

This work investigates the degradation of the electrical performance at STC of PV modules base on an innovative organic material (perovskite). The paper presents results for four PSCs using data collected in 2022 at Torino (Italy, with latitude of 45° North). In particular, a measurement station installed on the roof of a research lab permits to make the modules operate in the neighbourhood of their maximum power point and to periodically trace their *I-V* curves. Since such modules were prototypes, their electrical performance at STC was determined in the first day of the campaign, and they had comparable rated power and rated efficiency (≈0.81 W and ≈14%, respectively). Data from the experimental campaign were properly filtered

to exclude curves affected by mismatch, measurement errors or other issues (about 80% of the total curves). Filtered data were processed to quantify degradation of maximum power and efficiency over the experimental campaign. PV modules under test had different degradation rate, which ranged between ≈-51% and ≈-17%. The module with the lowest degradation had the lowest stress since its *I-V* curves were acquired in the shortest time interval (30 s). On the contrary, the module with the highest degradation was subject to the highest stress since its *I-V* curves were acquired in the longest interval (about 2 min) in two subsequent directions. Finally, the temperature coefficients for power were estimated, being comparable with the values generally provided for crystalline silicon modules. However, the obtained coefficients exhibit higher deviations within the same lot of production, in the range from - 0.407 %/°C to - 0.245 %/°C, instead of c-Si modules belonging to the same technology, with almost constant temperature coefficient. These results confirm that perovskite technology still needs improvements to allow commercial deployment. In the future, further experimental campaigns on new prototypal devices will be conducted to monitor their competitiveness with respect to c-Si modules.

REFERENCES

[1] A. Ciocia, P. Di Leo, S. Fichera, F. Giordano, G. Malgaroli, and F. Spertino, "A novel procedure to adjust the equivalent circuit parameters of photovoltaic modules under shading," *2020 International Symposium on Power Electronics, Electrical Drives, Automation and Motion, SPEEDAM 2020*, pp. 711–715, Jun. 2020, doi: 10.1109/SPEEDAM48782.2020.9161878.

[2] F. Bizzarri, S. Nitti, and G. Malgaroli, "The use of drones in the maintenance of photovoltaic fields," *E3S Web of Conferences*, vol. 119, Sep. 2019, doi: 10.1051/E3SCONF/201911900021.

[3] A. Carullo *et al.*, "Comparison of correction methods of wind speed for performance evaluation of wind turbines," *24th IMEKO TC4 International Symposium and 22nd International Workshop on ADC and DAC Modelling and Testing*, pp. 291–296, 2020.

[4] A. Amato, A. Ciocia, E. Garello, G. Malgaroli, and F. Spertino, "Hourly Simulation of Energy Community with Photovoltaic Generator and Electric Vehicle," *2022 IEEE International Conference on Environment and Electrical Engineering and 2022 IEEE Industrial and Commercial Power Systems Europe, EEEIC / I and CPS Europe 2022*, 2022, doi: 10.1109/EEEIC/ICPSEUROPE54979.2022.9854521.

[5] G. Antonetto *et al.*, "Synergistic freshwater and electricity production using passive membrane distillation and waste heat recovered from camouflaged photovoltaic modules," *J Clean Prod*, vol. 318, Oct. 2021, doi: 10.1016/J.JCLEPRO.2021.128464.

[6] A. Amato, M. Bilardo, E. Fabrizio, V. Serra, and F. Spertino, "Energy evaluation of a PV-based test facility for assessing future self-sufficient buildings," *Energies (Basel)*, vol. 14, no. 2, Jan. 2021, doi: 10.3390/EN14020329.

[7] "ITRPV 2021".

[8] L. C. Andreani, A. Bozzola, P. Kowalczewski, M. Liscidini, and L. Redorici, "Silicon solar cells: Toward the efficiency limits," *Advances in Physics: X*, vol. 4, no. 1. Taylor and Francis Ltd., Jan. 01, 2019. doi: 10.1080/23746149.2018.1548305.

[9] B. Ehrler, E. Alarcón-Lladó, S. W. Tabernig, T. Veeken, E. C. Garnett, and A. Polman, "Photovoltaics reaching for the shockley-queisser limit," *ACS Energy Lett*, vol. 5, no. 9, pp. 3029–3033, Sep. 2020, doi: 10.1021/acsenergylett.0c01790.

[10] L. Xu *et al.*, "Potential-induced degradation in perovskite/silicon tandem photovoltaic modules," *Cell Rep Phys Sci*, vol. 3, no. 9, Sep. 2022, doi: 10.1016/j.xcrp.2022.101026.

[11] N. G. Park, "Perovskite solar cells: An emerging photovoltaic technology," *Materials Today*, vol. 18, no. 2. Elsevier B.V., pp. 65–72, Mar. 01, 2015. doi: 10.1016/j.mattod.2014.07.007.

[12] Y. Jiang *et al.*, "Post-annealing of MAPbI3 perovskite films with methylamine for efficient perovskite solar cells†," *Mater Horiz*, vol. 3, no. 6, pp. 548–555, Nov. 2016, doi: 10.1039/c6mh00160b.

[13] Z. Chen *et al.*, "Single-Crystal MAPbI3 Perovskite Solar Cells Exceeding 21% Power Conversion Efficiency," *ACS Energy Lett*, vol. 4, no. 6, pp. 1258–1259, Jun. 2019, doi: 10.1021/acsenergylett.9b00847.

[14] N. Suresh Kumar and K. Chandra Babu Naidu, “A review on perovskite solar cells (PSCs), materials and applications,” *Journal of Materiomics*, vol. 7, no. 5, pp. 940–956, Sep. 2021, doi: 10.1016/j.jmat.2021.04.002.

[15] A. Tooghi, D. Fathi, and M. Eskandari, “High-performance perovskite solar cell using photonic–plasmonic nanostructure,” *Sci Rep*, vol. 10, no. 1, Dec. 2020, doi: 10.1038/s41598-020-67741-9.

[16] H. Liang, F. Wang, Z. Cheng, C. Xu, G. Li, and Y. Shuai, “Full-Spectrum Solar Energy Utilization and Enhanced Solar Energy Harvesting via Photon Anti-Reflection and Scattering Performance Using Nanophotonic Structure,” *ES Energy & Environment*, 2020, doi: 10.30919/esee8c456.

[17] H. S. Jung and N. G. Park, “Perovskite solar cells: From materials to devices,” *Small*, vol. 11, no. 1. Wiley-VCH Verlag, pp. 10–25, Jan. 07, 2015. doi: 10.1002/smll.201402767.

[18] J. Tong *et al.*, “High-performance methylammonium-free ideal-band-gap perovskite solar cells,” *Matter*, vol. 4, no. 4, pp. 1365–1376, Apr. 2021, doi: 10.1016/j.matt.2021.01.003.

[19] B. Chen *et al.*, “Enhanced optical path and electron diffusion length enable high-efficiency perovskite tandems,” *Nat Commun*, vol. 11, no. 1, Dec. 2020, doi: 10.1038/s41467-020-15077-3.

[20] M. Cai, Y. Wu, H. Chen, X. Yang, Y. Qiang, and L. Han, “Cost-Performance Analysis of Perovskite Solar Modules,” *Advanced Science*, vol. 4, no. 1, Jan. 2017, doi: 10.1002/advs.201600269.

[21] J. A. Christians, S. N. Habisreutinger, J. J. Berry, and J. M. Luther, “Stability in Perovskite Photovoltaics: A Paradigm for Newfangled Technologies,” *ACS Energy Letters*, vol. 3, no. 9. American Chemical Society, pp. 2136–2143, Sep. 14, 2018. doi: 10.1021/acsenergylett.8b00914.

[22] K. Ramspeck *et al.*, “Light Induced Degradation of Rear Passivated mc-Si Solar Cells APCVD SiO2 View project Minority carrier lifetime View project LIGHT INDUCED DEGRADATION OF REAR PASSIVATED MC-SI SOLAR CELLS,” 2012, doi: 10.4229/27thEUPVSEC2012-2DO.3.4.

[23] B. G. Krishna, D. Sundar Ghosh, and S. Tiwari, “Progress in ambient air-processed perovskite solar cells: Insights into processing techniques and stability assessment,” *Solar Energy*, vol. 224. Elsevier Ltd, pp. 1369–1395, Aug. 01, 2021. doi: 10.1016/j.solener.2021.07.002.

[24] M. V. Khenkin *et al.*, “Consensus statement for stability assessment and reporting for perovskite photovoltaics based on ISOS procedures,” *Nat Energy*, vol. 5, no. 1, pp. 35–49, Jan. 2020, doi: 10.1038/s41560-019-0529-5.

[25] F. De Rossi *et al.*, “An Interlaboratory Study on the Stability of All-Printable Hole Transport Material–Free Perovskite Solar Cells,” *Energy Technology*, vol. 8, no. 12, Dec. 2020, doi: 10.1002/ente.202000134.